

# TEMPORAL-AWARE REFINEMENT FOR VIDEO-BASED HUMAN POSE AND SHAPE RECOVERY

A PREPRINT

 **Ming Chen\***

Kuaishou Technology Co., Ltd.  
chenming09@kuaishou.com

 **Yan Zhou\***

Kuaishou Technology Co., Ltd.  
zhouyan03@kuaishou.com

 **Weihua Jian**

Kuaishou Technology Co., Ltd.  
jianweihua@kuaishou.com

 **Pengfei Wan**

Kuaishou Technology Co., Ltd.  
wanpengfei@kuaishou.com

 **Zhongyuan Wang**

Kuaishou Technology Co., Ltd.  
wangzhongyuan@kuaishou.com

November 17, 2023

## ABSTRACT

Though significant progress in human pose and shape recovery from monocular RGB images has been made in recent years, obtaining 3D human motion with high accuracy and temporal consistency from videos remains challenging. Existing video-based methods tend to reconstruct human motion from global image features, which lack detailed representation capability and limit the reconstruction accuracy. In this paper, we propose a Temporal-Aware Refining Network (TAR), to synchronously explore temporal-aware global and local image features for accurate pose and shape recovery. First, a global transformer encoder is introduced to obtain temporal global features from static feature sequences. Second, a bidirectional ConvGRU network takes the sequence of high-resolution feature maps as input, and outputs temporal local feature maps that maintain high resolution and capture the local motion of the human body. Finally, a recurrent refinement module iteratively updates estimated SMPL parameters by leveraging both global and local temporal information to achieve accurate and smooth results. Extensive experiments demonstrate that our TAR obtains more accurate results than previous state-of-the-art methods on popular benchmarks, i.e., 3DPW, MPI-INF-3DHP, and Human3.6M.

**Keywords** Human Pose and Mesh Recovery

## 1 Introduction

Monocular RGB image-based human pose and shape recovery is crucial in AR/VR, motion analysis, computer games, and human-computer interaction. In recent years, various image-based methods Kanazawa et al. [2018] Kolotouros et al. [2019a] Kocabas et al. [2021a] Wang and Daniilidis [2023] are proposed to tackle recovering human pose and shape from RGB images. Some methods directly estimate the parameters of a parametric model (e.g., SMPL Loper et al. [2015]), while others reconstruct the vertex coordinates of the human body surface.

Despite impressive improvements in image-based methods, capturing temporal-consistent human motion remains challenging. Video-based methods have been proposed to address this issue. Previous video-based methods typically design a network to model the long-term or local-temporal relations among global feature sequences of low-resolution extracted by a pretrained backbone Kolotouros et al. [2019a]. For instance, TCMR Choi et al. [2021] and GLoT Shen et al. [2023] consist of a GRU-based and Transformer-based temporal encoder, respectively. Although video-based methods have made progress improving intra-frame accuracy and inter-frame consistency, they still struggle to achieve the high accuracy of image-based counterparts. Most previous video-based methods generally focus on modeling global

\*Equal contributions

Figure 1: Previous methods TCMRChoi et al. [2021](white) and GLoTShen et al. [2023](purple) solely focus on leveraging global image features, which leads to inaccurate and misaligned meshes. In contrast, TAR(brown) modeling both global and local temporal information to capture more accurate human motion. *This is a video figure that is best viewed by Adobe Reader.*

features processed by the pooling operation of CNN backbones, neglecting critical local image features that contain detailed information on human pose and shape. Besides, these methods apply weakly-perspective assumption used in Kanazawa et al. [2018], which is not suitable in many real scenarios and leads to undesirable results.

To address the issues mentioned above, we propose the Temporal-Aware Refining Network (TAR) that utilizes temporal-aware global and local image features with a iterative regression module. Our method consists of a Global Temporal Encoder, a Local Temporal Encoder, and a Recurrent Refinement Module. The Global Temporal Encoder responses for temporal global information encoding with a 4-layer transformer encoder. The Local Temporal Encoder comprises a bidirectional ConvGRUs and focuses on modeling the dynamics of local image features. To fully utilize temporal features of different semantic levels, we propose a Recurrent Refinement Module that iteratively integrates local and global features to update predictions. Besides, we leverage full-image perspective camera model in the training phase to overcome the shortage of weakly perspective assumptionLi et al. [2022]. With these designs, TAR outperforms previous state-of-the-art methods on public 3DPW, MPI-INF-3DHP, and Human3.6M datasets. In summary, our contributions are as followed:

- We propose a Tempora-Aware Refining Network (TAR) for recovering 3D human mesh from video. TAR collaboratively exploits temporal global and local image features with Global and Local Temporal Encoders, achieving accurate and temporally consistent results.
- We propose a Recurrent Refinement Module to iteratively leverage temporal-aware global and local image features to refine predicted SMPL parameters.
- We conduct extensive experiments on three public datasetsVon Marcard et al. [2018]Ionescu et al. [2013]Mehta et al. [2017]. The results show that TAR surpasses the performance of previous methods. In addition, we also verify the generalization ability of TAR on the recent challenging dataset EMDBKaufmann et al. [2023].

## 2 Related Work

### 2.1 Image-based human pose and shape recovery.

3D human mesh recovery aims to reconstruct 3D human pose and shape from monocular images. Previous image-based methods can be divided into parametric methods and non-parametric methods. The first type estimates parameters of parametric human model (e.g., SMPLLoper et al. [2015]), while the second type reconstructs mesh vertices of human body. Early worksKanazawa et al. [2018]Kolotouros et al. [2019a]Kocabas et al. [2021b] directly predict SMPL pose and shape parameters from global image features extracted by pretrained CNNsHe et al. [2016]. However, they struggle

to generate accurate results due to the limited representation capability of global features. Recent worksKocabas et al. [2021a]Zhang et al. [2021]Wang and Daniilidis [2023] leverage local image features to complement the representation ability of global features and achieve better accuracy. Several worksLi et al. [2021]Li et al. [2023a]Song et al. [2020]Georgakis et al. [2020]Ma et al. [2023] employ intermediate representations and multiple stages to simplify parameters estimation. For example, HybriKLi et al. [2021] conducts swing-twist decomposition to joint rotations, breaking the task into two phases: detecting 3D keypoints and joint twists from images and computing poses via inverse kinematics. Other worksChoi et al. [2020]Moon and Lee [2020]Kolotouros et al. [2019b]Lin et al. [2021a]Lin et al. [2021b]Cho et al. [2022] directly predict 3D coordinates of mesh vertices from imagesKolotouros et al. [2019b]Lin et al. [2021a]Lin et al. [2021b]Cho et al. [2022] or 2D keypointsChoi et al. [2020]Moon and Lee [2020] to overcome the limited pose and shape representation space of SMPL model. Although image-based methods have made remarkable progress in accuracy, generating temporally consistent human motion from videos remains an open problem.

## 2.2 Video-based human pose and shape recovery.

Video-based methods aim to produce accurate and temporal-consistent human mesh from sequential video frames. Most methodsKocabas et al. [2020]Choi et al. [2021]Wei et al. [2022]Shen et al. [2023]Luo et al. [2020] use a pretrained CNNKolotouros et al. [2019a] to first extract static global features from image sequences and build temporal encoder such as attentionWei et al. [2022], GRUsKocabas et al. [2020]Choi et al. [2021] and TransformersShen et al. [2023], to predict SMPL parameters. Other methodsWan et al. [2021]Yang et al. [2023] train a Vision TransformerDosovitskiy et al. [2020] to extract fine-grained image features and exploit spatial-temporal relations from input sequences. MAEDWan et al. [2021] takes the image patch sequence as input and uses a spatial-temporal Transformer framework to predict SMPL parameters. INTYang et al. [2023] first trains a ViTDosovitskiy et al. [2020] to learn disentangled pose tokens from images and uses multiple temporal Transformers to capture the motion of each token. Despite the promising results of video-based methods, these methods only consider the global image features while discarding detailed spatial information, leading to trade-off between accuracy and smoothness. In contrast, our method simultaneously utilize temporal-aware local and global image features, achieving better per-frame accuracy and temporal consistency.

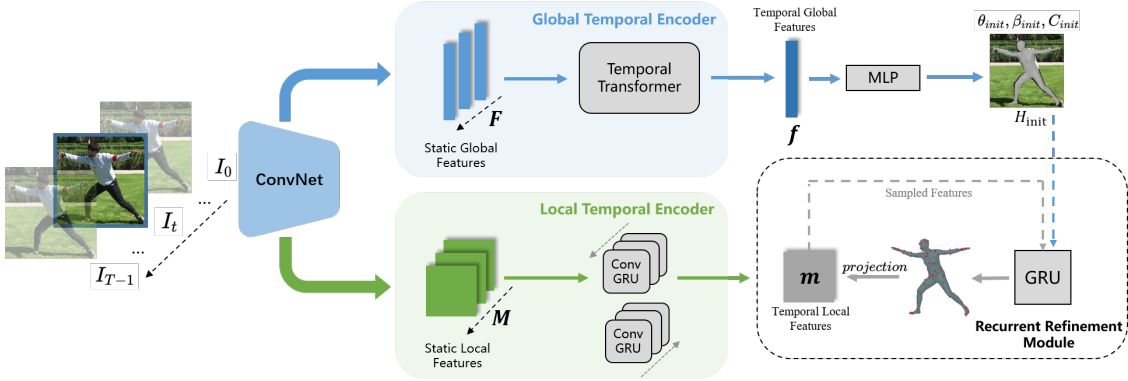


Figure 2: An overview of the proposed TAR. Given a sequence of images, static global features and local features are first extracted by a pretrained CNNHe et al. [2016]Wang et al. [2020]. Then a transformer-basedVaswani et al. [2017] Global Temporal Encoder takes the static global features  $\mathbf{F}$  as input and obtains temporal global features  $\mathbf{f}$  of the mid-frame, which is further converted to initial SMPL parameters and hidden states  $\mathbf{H}_{init}$  by a MLP network. Parallely, a Local Temporal Encoder composed of a bidirectional ConvGRUSiam et al. [2017] network extracts temporal local features  $\mathbf{m}$  from the static local features  $\mathbf{M}$ . Last, Recurrent Refinement Module initialized by  $\mathbf{H}_{init}$  utilizes  $\mathbf{f}$  and  $\mathbf{m}$  to iteratively update the estimated SMPL parameters.

## 3 Method

Figure 2 shows an overview of our Temporal-Aware Refining Network (TAR). TAR comprises three components: (1) A Global Temporal Encoder (GTE), (2) a Local Temporal Encoder (LTE) and (3) a Recurrent Refinement Module (RRM). Given an image sequence  $\mathbf{I}$  of length  $T$ ,  $\mathbf{I} = \{I_t\}_0^{T-1}$ , we first use a pretrained CNNHe et al. [2016]Siam et al. [2017] to extract the image features. Differing from previous methods, in addition to the global features  $\mathbf{F} = \{f_t\}_0^{T-1}$ , we extract high-resolution (e.g.,  $64 \times 64$ ) local feature maps  $\mathbf{M} = \{m_t\}_0^{T-1}$  to capture the detailed spatial information. Static global and local features are used as input to produce temporal-aware global and local representations, denoted by

$\mathbf{f}$  and  $\mathbf{m}$ , respectively, by GTE and LTE. Finally, both types of features are fed to the RRM, which iteratively updates the estimated SMPL parameters of the mid-frame in the input sequence. We elaborate on each component of TAR as follows.

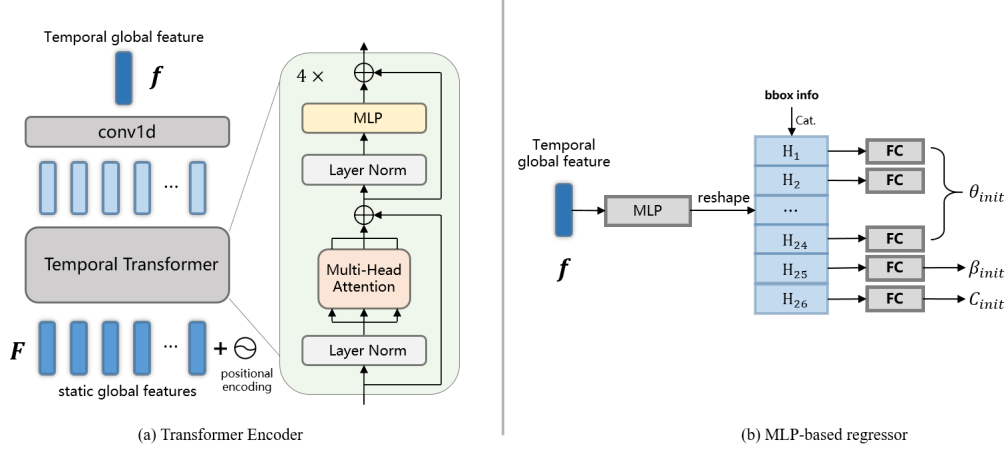


Figure 3: (a) Transformer encoder structure of Global Temporal Encoder and weighted average layer implemented with 1D convolution. (b) MLP-based regressor with 26 hidden states and bounding box information vector.

### 3.1 Global Temporal Encoder (GTE)

GTE involves two components, i.e. a temporal transformer encoder and an MLP-based regressor proposed by Wang and Daniilidis [2023]. The transformer encoder processes the static global features to obtain temporal-aware global features of the mid-frame. The regressor first converts the features into disentangled hidden states, which are latter used to regress the initial SMPL parameters.

#### 3.1.1 Transformer Encoder.

Transformers Vaswani et al. [2017] have shown a powerful capability to capture long-range global dependency of sequential data thanks to the self-attention mechanism. As shown in Figure 3(a), our GTE applies a 4-layer transformer encoder to learn the temporal consistency in human motion. Then a weighted average layer shrinks the entire sequence into a temporal global feature vector, which integrates historical and future information within the sequence.

#### 3.1.2 Initial Regressor.

After performing global temporal encoding, we estimate the SMPL Loper et al. [2015] parameters  $\Phi_{init} = \{\theta_{init}, \beta_{init}, C_{init}\}$ ,  $\theta_{init} \in \mathbb{R}^{24 \times 3}$ ,  $\beta_{init} \in \mathbb{R}^{10}$ ,  $C_{init} \in \mathbb{R}^3$  from the integrated temporal global features.  $\theta$  and  $\beta$  are pose and shape parameters that control the joint rotations and mesh shapes in SMPL, and  $C$  represents camera parameters Li et al. [2022] which project the 3D coordinates onto the full-image space. Instead of using the common iterative regressor proposed by HMR Kanazawa et al. [2018], we first convert the global features into 26 hidden states corresponding to 23 SMPL joint rotations, global orientation, shape coefficient and camera parameters. Together with bounding box information vector Li et al. [2022], all hidden states are sent to an MLP-based regressor to estimate SMPL parameters as shown in Figure 3(b). The hidden states and estimated parameters are subsequently used to initialize the Recurrent Refinement Module.

### 3.2 Local Temporal Encoder

The GTE integrates global features while disregarding essential local information in images, which has been proved beneficial for 3D accuracy and 2D alignment. As compensation, LTE exploits high-resolution representations with temporal awareness from static local feature maps to capture the local motion of human body.

#### 3.2.1 Convolutional Gated Recurrent Units.

ConvGRUs are widely used in video segmentation tasks Siam et al. [2017] Lin et al. [2022] to exploit temporal relations in high-resolution images. Inspired by this, we build the Local Temporal Encoder with a bidirectional ConvGRU network



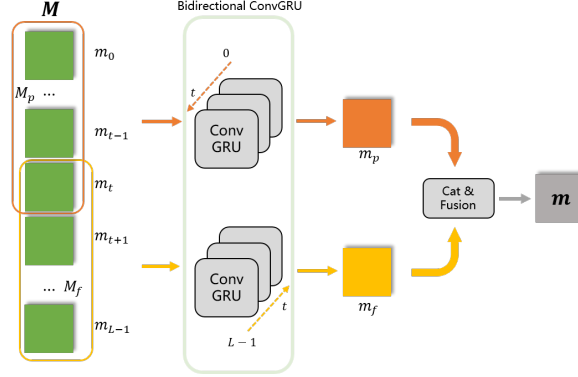


Figure 4: Local Temporal Encoder built with bidirectional ConvGRU.  $\mathbf{M}$  is a sequence local features with the shape of  $L \times D \times h \times w$ , where  $L$  is the size of local temporal window,  $D$  and  $(h, w)$  is the channel dimension and spatial resolution of local feature maps.  $\mathbf{m}_f$ ,  $\mathbf{m}_p$  are the outputs of history and future branch, respectively.  $\mathbf{m}$  is the final temporal-aware local features extracted by LTE.

to leverage both future and historical temporal information from local features. As shown in Figure 4, the sequence of local features  $\mathbf{M} = \{m_t\}_0^{L-1}$ ,  $m \in \mathbb{R}^{D \times h \times w}$  is first split into two parts  $\mathbf{M}_p = \{m_t\}_0^\tau$  and  $\mathbf{M}_f = \{m_t\}_{L-1}^\tau$ , where  $\tau = \lfloor (L-1)/2 \rfloor$  is the index of the mid-frame. Then, the bidirectional ConvGRU computes the hidden maps  $\mathbf{m}_p$ ,  $\mathbf{m}_f$  from both sub-sequences. In each ConvGRU block, the computation process can be written as

$$Z_t = \sigma(W_z * m_t + U_z * h_{t-1}) \quad (1)$$

$$R_t = \sigma(W_r * m_t + U_r * h_{t-1}) \quad (2)$$

$$\tilde{h}_t = \tanh(W * m_t + U * (R_t \circ h_{t-1})) \quad (3)$$

$$h_t = (1 - Z_t) \circ h_{t-1} + Z_t \circ \tilde{h}_t, \quad (4)$$

where  $h_t, h_{t-1}$  represent hidden maps of ConvGRU at different time steps, and  $W, U$  are learnable weights. The hidden maps  $h$  have the same shape with input local features  $m_t$  and are initialized with zeros in both branches. Last, a convolutional layer concatenates and projects the hidden maps  $\mathbf{m}_f, \mathbf{m}_p$  into the temporal-aware local features  $\mathbf{m}$ .

It is worth noting that, the size of window  $L$  of LTE can be different from length  $T$  of input sequence, and we empirically find that LTE benefits from smaller  $L$  than  $T$ . We assume the reason is that ConvGRU is more suitable for capturing local motion information in a short period instead of long-range modeling. The experiments in Session 4 verify the impact of  $L$ .

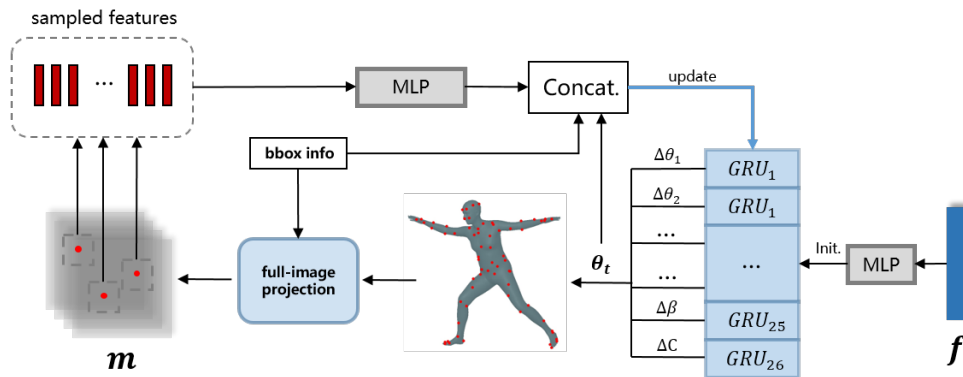


Figure 5: The proposed Recurrent Refinement Module. It contains 26 disentangled GRUs to update SMPL parameters with local features and bounding box information.

### 3.3 Recurrent Refinement Module

Previous video-based methods Kocabas et al. [2020] Choi et al. [2021] Wei et al. [2022] Shen et al. [2023] generally apply a regressor to estimate SMPL parameters from temporal global features without utilizing local image details. Inspired by

recent image-based methodsZhang et al. [2021]Wang and Daniilidis [2023], we propose Recurrent Refinement Module (RRM) to update estimated parameters with collaborative usage of temporal local and global features. Specifically, we build 26 disentangled GRUs to update SMPL poses, shape and camera parameters. In each iteration  $l$ , the GRUs take feedback signal  $\mathbf{s}_l$  as input, and predicts an update step  $\Delta\Phi_l$ , which is added to produce the next estimation:  $\Phi_{l+1} = \Phi_l + \Delta\Phi_l$ .

### 3.3.1 Feedback Signal.

Given the initial estimate  $\Phi_{init}$  from GTE, we first obtain the SMPL mesh via forward kinematics and linear blend shapesLoper et al. [2015]. Following Wang and Daniilidis [2023],  $K$  markers  $\mathbf{J} = \{J_k = (x_k, y_k, z_k)\}_{k=1}^{K=26}$  are sampled from the SMPL mesh and projected and transformed to bounding box space to get  $K$  keypoints  $\mathbf{j} = \{j_k = (u_k, v_k)\}_{k=1}^{K=26}$ . As proposed in CLIFFLi et al. [2022], we conduct the more reasonable full-image projection instead of the widely used weakly-perspective projection:

$$j_k^{full} = \Pi(J_k + t^{full}) \quad (5)$$

$$j_k = (j_k^{full} - c^{bbox}) / s^{bbox} \quad (6)$$

where  $t^{full}$  is the translation with respect to the optical center of the full image, which is estimated from camera parameters  $CLi et al. [2022]$ .  $c^{bbox}$  and  $s^{bbox}$  are the center and size of the bounding box from which the crop is obtained. For each  $j_k$ , we take the feature values inside a window centered at  $j_k$  as

$$s_k = \{g(j) \in \mathbf{m} \mid \|j - j_k\| \leq r\} \quad (7)$$

where we set  $r = 3$  pixels as the radius of the window. We then concatenate sampled feature values of all the markers, along with current estimate  $\Phi_l$  and bounding box information vector  $v^{cliff}$  proposed in Li et al. [2022] to form the feedback signal:

$$\mathbf{s}_l = [s_1, \dots, s_K, \Phi_l, v^{cliff}] \quad (8)$$

### 3.3.2 Update Step.

Once the feedback signal  $\mathbf{s}_l$  is obtained, the hidden states of all GRUs are updated parallelly:

$$h_n^{l+1} \leftarrow (h_n^l, \mathbf{s}_l), n = 1, \dots, 26 \quad (9)$$

and 26 individual regressors map the hidden states to update step  $\Delta\Phi_l$ . There are two major differences between RRM and the feedback module in Wang and Daniilidis [2023]. First, the hidden states of GRUs are initialized with global temporal features, which is zero-initialized in Wang and Daniilidis [2023] instead. Second, our RRM sampled from temporal-aware local features, capturing more temporal dynamics of human body compared to the static features used inWang and Daniilidis [2023]. These two differences promote our method to capture smoother and more accurate human motion.

## 3.4 Loss Functions

Following previous methodsChoi et al. [2021]Wei et al. [2022], we impose  $L_2$  loss between the estimated and ground truth SMPL parameters and 2D/3D joint coordinates to supervise the initial results of all update stages in GTE and RRM:

$$L_l = \lambda_{2D} L_{2D}^l + \lambda_{3D} L_{3D}^l + \lambda_{SMPL} L_{SMPL}^l \quad (10)$$

$$L_{2D}^l = \|\hat{\mathbf{J}}_{2D} - \mathbf{J}_{2D}^l\|_F^2 \quad (11)$$

$$L_{3D}^l = \|\hat{\mathbf{J}}_{3D} - \mathbf{J}_{3D}^l\|_F^2 \quad (12)$$

$$L_{SMPL}^l = \|\hat{\theta} - \theta^l\|_F^2 + \|\hat{\beta} - \beta^l\|_F^2 \quad (13)$$

the hat operator denotes the ground truth of that variable. The final loss is a weighted sum of the loss at each iterative update and initial state

$$L = \sum_{l=0}^L \gamma^{L-l} L_l \quad (14)$$

where we set  $\gamma=0.85$  and  $L=5$  for all experiments following Wang and Daniilidis [2023]. To be noted, our model only estimate the parameters at the mid-frame of the sequence.

## 4 Experiments

We first introduce the evaluation metrics and datasets. Next, we report the evaluation results of our method and comparison with previous methods. Finally, we provide ablation studies to prove the effectiveness of the proposed method.

### 4.0.1 Evaluation Metrics.

Following previous methods Choi et al. [2021] Wei et al. [2022] Shen et al. [2023], we report results in the metrics of intra-frame accuracy temporal consistency. For intra-frame metrics, we adopt Mean Per Joint Position Error (MPJPE), Procrustes-aligned MPJPE (PA-MPJPE), and Mean Per Vertex Position Error (MPVPE). For temporal consistency, we report acceleration error (ACCEL) to verify inter-frame smooth.

### 4.0.2 Datasets.

We adopt mixed 2D and 3D datasets for training. For 3D datasets, we use 3DPW Von Marcard et al. [2018], Human3.6M Ionescu et al. [2013] and MPI-INF-3DHP Mehta et al. [2017], which contain annotations of SMPL parameters or 3D joints. We do not use MoshLoper et al. [2014] data of Human3.6M, instead we use the pseudo ground truth from NeuralAnnot Moon et al. [2022]. For 2D datasets, we use COCO Lin et al. [2014] and MPII Andriluka et al. [2014], which contain 2D joint annotations and pseudo SMPL parameters fitted by EFTJoo et al. [2021]. Since COCO and MPII are both image-based datasets, we repeat each image  $T$  times to form a sequence for training. For evaluation, we use the test set of 3DPW, Human3.6M and MPI-INF-3DHP. Additionally, we evaluate our method on a new challenging 3D dataset EMBD Kaufmann et al. [2023] to demonstrate the generalization performance.

### 4.1 Comparison with state-of-the-art methods

Table 1: Evaluation of state-of-the-art methods on 3DPW, MPI-INF-3DHP, and Human3.6M datasets. All Methods use 3DPW training set in training phase. † and \* represent using HRNet Wang et al. [2020] and ResNet50 He et al. [2016] backbone, respectively. **Bold**: best; Underline: second best.

Method	3DPW				MPI-INF-3DHP			Human3.6M			Number of input frames
	MPJPE↓	PA-MPJPE↓	PVE↓	ACCEL↓	MPJPE↓	PA-MPJPE↓	ACCEL↓	MPJPE↓	PA-MPJPE↓	ACCEL↓	
VIBE Kocabas et al. [2020]	91.9	57.6	99.1	25.4	103.9	68.9	27.3	65.9	41.5	18.3	16
MEVA Luo et al. [2020]	86.9	54.7	-	11.6	96.4	65.4	11.1	76.0	53.2	15.3	90
TCMR Choi et al. [2021]	86.5	52.7	102.9	<u>7.1</u>	97.6	63.5	<u>8.5</u>	62.3	41.1	<u>5.3</u>	16
MAED Wan et al. [2021]	79.1	45.7	92.6	17.6	<b>83.6</b>	<b>56.2</b>	-	56.4	38.7	-	64
MPS-Net Wei et al. [2022]	84.3	52.1	99.7	7.4	96.7	62.8	9.6	69.4	47.4	<b>3.6</b>	16
INT Yang et al. [2023]	75.6	<u>42.0</u>	87.9	16.5	-	-	-	54.9	38.4	-	64
GLoT Shen et al. [2023]	80.7	50.6	96.3	<b>6.6</b>	93.9	61.5	<b>7.9</b>	67.0	46.3	<b>3.6</b>	16
<b>TAR(Ours)*</b>	<u>68.4</u>	45.3	83.9	7.9	87.5	62.7	9.6	<u>53.1</u>	<u>37.8</u>	5.6	<b>9</b>
<b>TAR(Ours)†</b>	<b>62.7</b>	<b>40.6</b>	<b>74.4</b>	7.7	<u>85.9</u>	<u>60.5</u>	9.2	<b>45.6</b>	<b>33.3</b>	5.6	<b>9</b>

#### 4.1.1 Video-based methods.

Table 1 compares our method with the state-of-the-art video-based methods on 3DPW, MPI-INF-3DHP and Human3.6M datasets. Our TAR outperforms existing methods by a large margin on Human3.6M and challenging 3DPW in 3D accuracy metrics, and achieve comparable results on MPI-INF-3DHP dataset. Specifically, TAR brings 15.4mm and 9.3mm decrease of MPJPE on 3DPW and Human3.6M. Although previous methods, e.g., MPS-Net Wei et al. [2022] and GLoT Shen et al. [2023] achieve splendid inter-frame smoothness by temporal attention over static global features extracted by SPIN Kolotouros et al. [2019a], they ignore the detailed local features and use the inappropriate weakly-perspective assumption. Due to these drawbacks, these methods fail to perceive subtle motion of human body and produce large error in real scenario. MAED Wan et al. [2021] and INT Yang et al. [2023] train ViTDosovitskiy et al. [2020] as the backbone and take use of fine-grained feature maps to achieve more accurate results. Nevertheless, these methods are time-costing and memory-intensive since they require longer input sequence, e.g.,  $T=64$ . Moreover, these they fail to achieve temporal consistent results compared to other methods. In contrast, our method can estimate accurate and smooth human motion from video with a small input sequence  $T=9$ . The results demonstrate that exploiting

temporal local features and the recurrent refinement mechanism can effectively achieve high intra-frame accuracy and inter-frame consistency.

Table 2: Evaluation of state-of-the-art methods on 3DPW. All methods do not use 3DPW on training.

Method		3DPW			
		MPJPE↓	PA-MPJPE↓	MPVPE↓	ACCEL↓
image-based	HMRKanazawa et al. [2018]	130.0	76.7	-	37.4
	Pose2PoseMoon and Lee [2020]	86.6	54.4	-	-
	Pose2MeshChoi et al. [2020]	88.9	58.3	-	-
	SPINKolotouros et al. [2019a]	96.9	59.2	116.4	29.8
	PyMAFZhang et al. [2021]	78.0	47.1	91.3	-
	PAREKocabas et al. [2021a]	82.0	50.9	97.9	-
	HybrIKLi et al. [2021]	80.0	48.8	94.5	-
video-based	HMMRKanazawa et al. [2019]	116.5	72.6	139.3	15.2
	VIBEKocabas et al. [2020]	93.5	56.5	113.4	27.1
	TCMRChoi et al. [2021]	95.0	56.5	111.5	7.0
	MPS-NetWei et al. [2022]	91.6	54.0	109.6	7.5
	INTYang et al. [2023]	90.0	49.7	105.1	23.5
	GLoTShen et al. [2023]	89.9	53.5	107.8	<b>6.7</b>
	<b>TAR(Ours)</b>	<b>71.0</b>	<b>46.3</b>	<b>84.7</b>	7.4

#### 4.1.2 Image-based and video-based methods

We further compare our TAR with the previous image-based and video-based methods on the challenging in-the-wild 3DPW dataset. Notice that all methods did not use the 3DPW training set in the training phases. The evaluation results are demonstrated in Table 2. Our TAR outperforms existing methods on all intra-frame metrics, and also achieve comparable smoothness with state-of-the-art video-based methods. For example, TAR significantly surpasses previous single image-based and video-based methods by 9.0mm and 18.9mm on MPJPE metric. The results confirm that our proposed TAR is capable for capturing accurate and smooth motion from videos.

## 4.2 Ablation Study

### 4.2.1 Recurrent Refinement Module (RRM)

TAR collaboratively use temporal global and local features in a iterative manner. Without RRM, only temporal global features are used to estimate final results, i.e., the initial estimate  $\Phi_{init}$  in GTE. As shown in Table 3, the intra-frame accuracy dramatically degrades without RRM. The evaluation results verify that utilizing local features is crucial to improving 3D accuracy.

Table 3: Ablation study for Recurrent Refinement Module on 3DPW dataset.

Method	MPJPE↓	PA-MPJPE↓	PVE↓	ACCEL↓
w/o RRM	73.7	45.8	86.5	<b>6.8</b>
Ours	<b>62.7</b>	<b>40.6</b>	<b>74.4</b>	7.7

### 4.2.2 Global Temporal Encoder (GTE) and Local Temporal Encoder (LTE).

There are two temporal encoders in our TAR, i.e., Global Temporal Encoder and Local Temporal Encoder, to respectively capture temporal-aware global and local features from given input sequences. The evaluation results of temporal encoders are in Table 4. By removing LTE and GTE, the performance decreases in both intra-frame and inter-frame metrics, especially ACCEL. The GTE captures the motion by integrating global features, which is essential to the temporal perception ability. However, isolately using GTE is not sufficient for producing accurate and smooth results. The reason is that, in Recurrent Refining Module, local features are iteratively used to update the hidden states initialized by temporal global features. Without LTE, the local features are temporal-agnostic and will degrade the temporal awareness of global features from GTE. The results prove that both GTE and LTE are essential to our TAR.

Table 4: Ablation study for Global and Local Temporal Encoders on 3DPW dataset.

Method	MPJPE↓	PA-MPJPE↓	PVE↓	ACCEL↓
only GTE	66.7	41.8	78.5	16.0
only LTE	65.4	41.1	76.4	19.7
Both(Ours)	<b>62.7</b>	<b>40.6</b>	<b>74.4</b>	<b>7.7</b>

#### 4.2.3 Lengths of nearby frames of LTE.

As illustrated in Section 3, the size of window in LTE can be different from the input sequence. We evaluate the impact of different lengths of nearby frames of LTE. As shown in Table 5, we discover that the model achieves the best results when  $L=5$ . Although the estimation results gain better temporal consistency when the sequence gets longer, the 3D accuracy also degrades. We assume one probable reason is that ConvGRUs can effectively capture short-term local temporal features, while lacks sufficient modeling ability. Besides, the evaluation results reveal that even small sequences of local features lead to conspicuous temporal-consistency improvement, which proves the significance of temporal local features in TAR.

Table 5: Ablation study of different lengths of nearby frames of LTE. The length of 5 means 2 frames before and after the current frame.

Method	MPJPE↓	PA-MPJPE↓	PVE↓	ACCEL↓
L=3	64.9	42.1	77.4	9.0
<b>L=5</b>	<b>62.7</b>	<b>40.6</b>	<b>74.4</b>	<b>7.7</b>
L=7	64.7	42.1	77.3	<b>7.2</b>
L=9	66.4	42.5	79.1	7.3

### 4.3 Additional Experiment

#### 4.3.1 Evaluation on EMDB dataset

EMDBKaufmann et al. [2023] is a recently proposed electromagnetic dataset of 3D human pose and shape in the wild. It contains high-quality SMPL pose and shape parameters for in-the-wild videos. It contains a total of 58 minutes of motion data, distributed over 81 indoor and outdoor sequences and 10 participants, which are collected with body-worn, wireless electromagnetic (EM) sensors and a hand-held iPhone. Samples in EMDB are significantly different from commonly used datasets and are suitable for verifying the generalization of TAR. Following the split protocol in Kaufmann et al. [2023], we evaluate TAR on EMDB 1 in Table 6. Our TAR surpasses previous image-based methods on all metrics by a large margin. The results verify the generalization ability of TAR.

Table 6: Evaluation of state-of-the-art image-based methods and TAR on EMDB 1.

Method	MPJPE[mm]	PA-MPJPE[mm]	MVE[mm]	MVE-PA[mm]	MPJAE[deg]	MPJAE-PA[deg]	Jitter
PyMAFZhang et al. [2021]	131.1±54.9	82.9±38.2	160.0±64.5	98.1±44.4	28.5±12.5	25.7±10.1	81.8±25.6
PAREKocabas et al. [2021a]	113.9±49.5	72.2±33.9	133.2±57.4	85.4±39.1	24.7±9.8	22.4±8.8	75.1±22.5
CLIFFLi et al. [2022]	103.1±43.7	68.8±33.8	122.9±49.5	81.3±37.9	23.1±9.9	21.6±8.6	55.5±17.9
HybrIKLi et al. [2021]	103.0±44.3	65.6±33.3	122.2±50.5	80.4±39.1	24.5±11.3	23.1±11.1	49.2±18.5
TAR(Ours)	<b>89.4±48.0</b>	<b>58.9±35.0</b>	<b>102.7±53.2</b>	<b>69.3±38.9</b>	<b>21.5±15.2</b>	<b>21.4±17.4</b>	<b>12.0±6.6</b>

#### 4.3.2 Comparison with SmoothNet

SmoothNetZeng et al. [2022] shows remarkable performance in improving accuracy and smoothness of 2D/3D keypoints and human shape recovery models. It is method-agnostic and gains consistent improvements on public 3DPW dataset for image-based methodsKolotouros et al. [2019a]Kocabas et al. [2021a]. Since TAR is built on top of stronger

Table 7: Evaluation of ReFitWang and Daniilidis [2023], SmoothNetZeng et al. [2022] and TAR on 3DPW dataset. ‡ represents our implementation.

Method	MPJPE↓	PA-MPJPE↓	PVE↓	ACCEL↓
ReFitWang and Daniilidis [2023]‡	65.7	41.2	75.1	25.9
ReFitWang and Daniilidis [2023]‡+SmoothNetZeng et al. [2022](T=8)	<b>62.7</b>	41.3	<b>73.6</b>	12.1
ReFitWang and Daniilidis [2023]‡+SmoothNetZeng et al. [2022](T=16)	<b>62.7</b>	41.5	<b>73.6</b>	10.3
TAR(Ours)	<b>62.7</b>	<b>40.6</b>	74.4	<b>7.7</b>

base model than generally used SPINKolotouros et al. [2019a], we compare our method with SmoothNet and a recent state-of-the-art ReFitWang and Daniilidis [2023] to verify the performance in terms of accuracy and temporal-consistency of TAR. As shown in Table, our TAR achieves comparable 3D accuracy and surpassing smoothness with SmoothNet with larger window size. The evaluation further proves the effectiveness of TAR.



Figure 6: Visual comparison between GLoT (purple meshes) and our TAR (brown meshes) on the challenging 3DPW dataset. Our method can generate more plausible and image-aligned mesh results than GLoT.



Figure 7: Qualitative results of TAR on challenging EMDB dataset.



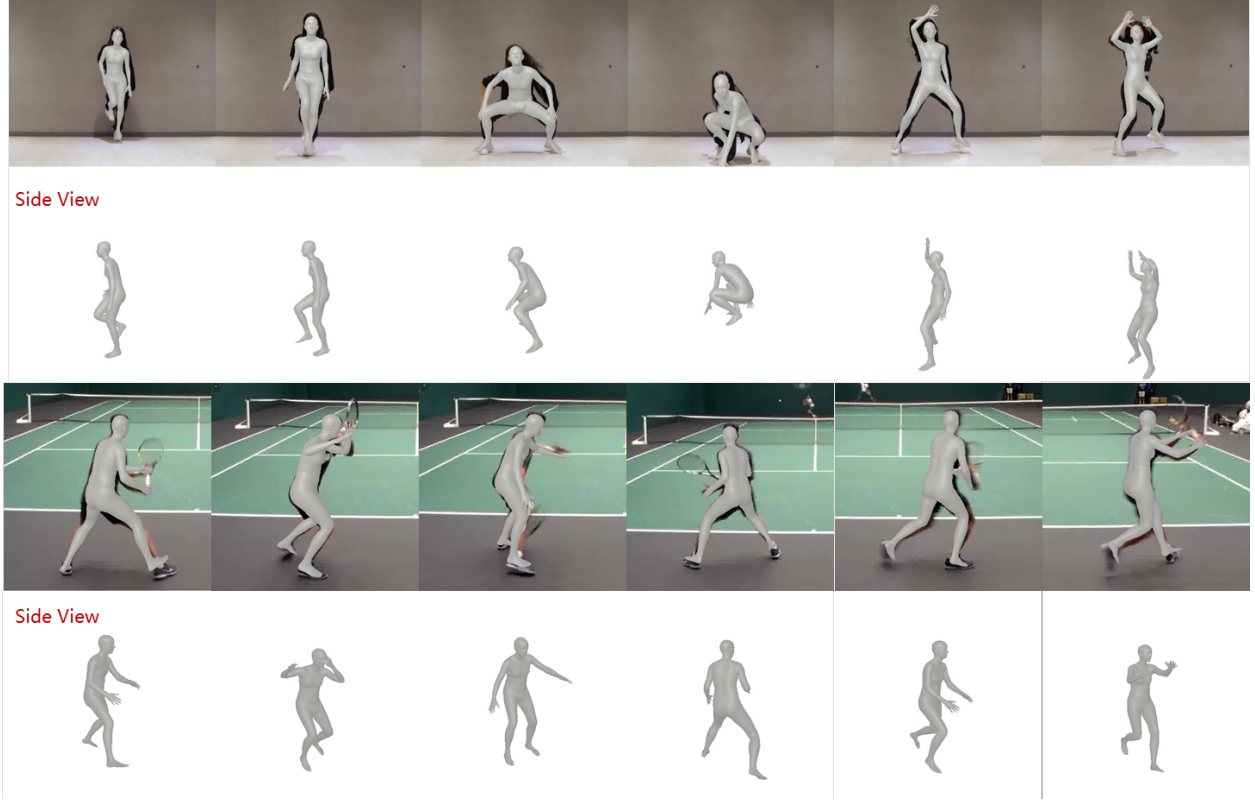


Figure 8: Qualitative results of TAR on challenging internet videos.

#### 4.4 Qualitative Evaluation

##### 4.4.1 Visual Comparison with GLoTShen et al. [2023].

Figure 6 shows the qualitative comparison between the previous state-of-the-art method GLoT and our TAR on the in-the-wild 3DPW dataset. Our method produces results with better 3D accuracy and better alignment with 2D images. Our method can achieve more reasonable results when an occlusion occurs (Row 1) by exploiting both temporal and spatial relations in a video sequence.

##### 4.4.2 Qualitative results on EMDB and internet videos.

Figure 7 shows the qualitative results on challenging EMDB dataset. Videos in EMDB dataset are recorded with a hand-held Iphone, which frequently violates the weakly projection assumption. Our TAR can generate smooth, accurate and well-aligned human meshes on EMDB videos. In Figure 8, we validate our method on challenging internet videos and provide rendered meshes of an side viewpoint. The results demonstrate that our TAR can handle challenging real scenarios.

## 5 Conclusions

This paper proposes a novel Temporal-Aware Refining Network (TAR) for video-based 3D human pose and shape recovery, which collaboratively exploits both temporal global and local features of videos with Global/Local Temporal Encoder and Recurrent Refinement Module. Extensive experiments demonstrate that TAR achieves state-of-the-art performance on three widely used datasets. Furthermore, TAR shows remarkable generalizing capability on challenging in-the-wild EMDB dataset and internet videos. We hope that our approach will spark further research in video-based 3D human pose and shape recovery.



### 5.1 Limitations.

Our method produces degraded result when the human body is highly occluded. The future work will explore the physical constraints and motion prior to further improve the performance. TAR is slightly inferior to SOTA video-based methods on inter-frame metric, which is our future optimization direction.

## References

- Hongsuk Choi, Gyeongsik Moon, Ju Yong Chang, and Kyoung Mu Lee. Beyond static features for temporally consistent 3d human pose and shape from a video. In *Proceedings of the IEEE/CVF conference on computer vision and pattern recognition*, pages 1964–1973, 2021.
- Xiaolong Shen, Zongxin Yang, Xiaohan Wang, Jianxin Ma, Chang Zhou, and Yi Yang. Global-to-local modeling for video-based 3d human pose and shape estimation. In *Proceedings of the IEEE/CVF Conference on Computer Vision and Pattern Recognition*, pages 8887–8896, 2023.
- Angjoo Kanazawa, Michael J Black, David W Jacobs, and Jitendra Malik. End-to-end recovery of human shape and pose. In *Proceedings of the IEEE conference on computer vision and pattern recognition*, pages 7122–7131, 2018.
- Nikos Kolotouros, Georgios Pavlakos, Michael J Black, and Kostas Daniilidis. Learning to reconstruct 3d human pose and shape via model-fitting in the loop. In *Proceedings of the IEEE/CVF international conference on computer vision*, pages 2252–2261, 2019a.
- Muhammed Kocabas, Chun-Hao P Huang, Otmar Hilliges, and Michael J Black. Pare: Part attention regressor for 3d human body estimation. In *Proceedings of the IEEE/CVF International Conference on Computer Vision*, pages 11127–11137, 2021a.
- Yufu Wang and Kostas Daniilidis. Refit: Recurrent fitting network for 3d human recovery. In *Proceedings of the IEEE/CVF International Conference on Computer Vision*, pages 14644–14654, 2023.
- Matthew Loper, Naureen Mahmood, Javier Romero, Gerard Pons-Moll, and Michael J. Black. SMPL: A skinned multi-person linear model. *ACM Trans. Graphics (Proc. SIGGRAPH Asia)*, 34(6):248:1–248:16, October 2015.
- Zhihao Li, Jianzhuang Liu, Zhensong Zhang, Songcen Xu, and Youliang Yan. Cliff: Carrying location information in full frames into human pose and shape estimation. In *European Conference on Computer Vision*, pages 590–606. Springer, 2022.
- Timo Von Marcard, Roberto Henschel, Michael J Black, Bodo Rosenhahn, and Gerard Pons-Moll. Recovering accurate 3d human pose in the wild using imus and a moving camera. In *Proceedings of the European conference on computer vision (ECCV)*, pages 601–617, 2018.
- Catalin Ionescu, Dragos Papava, Vlad Olaru, and Cristian Sminchisescu. Human3.6m: Large scale datasets and predictive methods for 3d human sensing in natural environments. *IEEE transactions on pattern analysis and machine intelligence*, 36(7):1325–1339, 2013.
- Dushyant Mehta, Helge Rhodin, Dan Casas, Pascal Fua, Oleksandr Sotnychenko, Weipeng Xu, and Christian Theobalt. Monocular 3d human pose estimation in the wild using improved cnn supervision. In *2017 international conference on 3D vision (3DV)*, pages 506–516. IEEE, 2017.
- Manuel Kaufmann, Jie Song, Chen Guo, Kaiyue Shen, Tianjian Jiang, Chengcheng Tang, Juan José Zárate, and Otmar Hilliges. Emdb: The electromagnetic database of global 3d human pose and shape in the wild. In *Proceedings of the IEEE/CVF International Conference on Computer Vision*, pages 14632–14643, 2023.
- Muhammed Kocabas, Chun-Hao P Huang, Joachim Tesch, Lea Müller, Otmar Hilliges, and Michael J Black. Spec: Seeing people in the wild with an estimated camera. In *Proceedings of the IEEE/CVF International Conference on Computer Vision*, pages 11035–11045, 2021b.
- Kaiming He, Xiangyu Zhang, Shaoqing Ren, and Jian Sun. Deep residual learning for image recognition. In *Proceedings of the IEEE conference on computer vision and pattern recognition*, pages 770–778, 2016.
- Hongwen Zhang, Yating Tian, Xinchu Zhou, Wanli Ouyang, Yebin Liu, Limin Wang, and Zhenan Sun. Pymaf: 3d human pose and shape regression with pyramidal mesh alignment feedback loop. In *Proceedings of the IEEE/CVF International Conference on Computer Vision*, pages 11446–11456, 2021.
- Jiefeng Li, Chao Xu, Zhicun Chen, Siyuan Bian, Lixin Yang, and Cewu Lu. Hybrik: A hybrid analytical-neural inverse kinematics solution for 3d human pose and shape estimation. In *Proceedings of the IEEE/CVF conference on computer vision and pattern recognition*, pages 3383–3393, 2021.
- Jiefeng Li, Siyuan Bian, Qi Liu, Jiasheng Tang, Fan Wang, and Cewu Lu. Niki: Neural inverse kinematics with invertible neural networks for 3d human pose and shape estimation. In *Proceedings of the IEEE/CVF Conference on Computer Vision and Pattern Recognition*, pages 12933–12942, 2023a.
- Jie Song, Xu Chen, and Otmar Hilliges. Human body model fitting by learned gradient descent. In *European Conference on Computer Vision*, pages 744–760. Springer, 2020.
- Georgios Georgakis, Ren Li, Srikrishna Karanam, Terrence Chen, Jana Košecká, and Ziyang Wu. Hierarchical kinematic human mesh recovery. In *Computer Vision–ECCV 2020: 16th European Conference, Glasgow, UK, August 23–28, 2020, Proceedings, Part XVII 16*, pages 768–784. Springer, 2020.

- Xiaoxuan Ma, Jiajun Su, Chunyu Wang, Wentao Zhu, and Yizhou Wang. 3d human mesh estimation from virtual markers. In *Proceedings of the IEEE/CVF Conference on Computer Vision and Pattern Recognition*, pages 534–543, 2023.
- Hongsuk Choi, Gyeongsik Moon, and Kyoung Mu Lee. Pose2mesh: Graph convolutional network for 3d human pose and mesh recovery from a 2d human pose. In *Computer Vision–ECCV 2020: 16th European Conference, Glasgow, UK, August 23–28, 2020, Proceedings, Part VII 16*, pages 769–787. Springer, 2020.
- Gyeongsik Moon and Kyoung Mu Lee. Pose2pose: 3d positional pose-guided 3d rotational pose prediction for expressive 3d human pose and mesh estimation. *arXiv preprint arXiv:2011.11534*, 1(2), 2020.
- Nikos Kolotouros, Georgios Pavlakos, and Kostas Daniilidis. Convolutional mesh regression for single-image human shape reconstruction. In *Proceedings of the IEEE/CVF Conference on Computer Vision and Pattern Recognition*, pages 4501–4510, 2019b.
- Kevin Lin, Lijuan Wang, and Zicheng Liu. Mesh graphormer. In *Proceedings of the IEEE/CVF international conference on computer vision*, pages 12939–12948, 2021a.
- Kevin Lin, Lijuan Wang, and Zicheng Liu. End-to-end human pose and mesh reconstruction with transformers. In *Proceedings of the IEEE/CVF conference on computer vision and pattern recognition*, pages 1954–1963, 2021b.
- Junhyeong Cho, Kim Youwang, and Tae-Hyun Oh. Cross-attention of disentangled modalities for 3d human mesh recovery with transformers. In *European Conference on Computer Vision*, pages 342–359. Springer, 2022.
- Muhammed Kocabas, Nikos Athanasiou, and Michael J Black. Vibe: Video inference for human body pose and shape estimation. In *Proceedings of the IEEE/CVF conference on computer vision and pattern recognition*, pages 5253–5263, 2020.
- Wen-Li Wei, Jen-Chun Lin, Tyng-Luh Liu, and Hong-Yuan Mark Liao. Capturing humans in motion: Temporal-attentive 3d human pose and shape estimation from monocular video. In *Proceedings of the IEEE/CVF Conference on Computer Vision and Pattern Recognition*, pages 13211–13220, 2022.
- Zhengyi Luo, S Alireza Golestaneh, and Kris M Kitani. 3d human motion estimation via motion compression and refinement. In *Proceedings of the Asian Conference on Computer Vision*, 2020.
- Ziniu Wan, Zhengjia Li, Maoqing Tian, Jianbo Liu, Shuai Yi, and Hongsheng Li. Encoder-decoder with multi-level attention for 3d human shape and pose estimation. In *Proceedings of the IEEE/CVF International Conference on Computer Vision*, pages 13033–13042, 2021.
- Sen Yang, Wen Heng, Gang Liu, Guozhong Luo, Wankou Yang, and Gang Yu. Capturing the motion of every joint: 3d human pose and shape estimation with independent tokens. *arXiv preprint arXiv:2303.00298*, 2023.
- Alexey Dosovitskiy, Lucas Beyer, Alexander Kolesnikov, Dirk Weissenborn, Xiaohua Zhai, Thomas Unterthiner, Mostafa Dehghani, Matthias Minderer, Georg Heigold, Sylvain Gelly, et al. An image is worth 16x16 words: Transformers for image recognition at scale. *arXiv preprint arXiv:2010.11929*, 2020.
- Jingdong Wang, Ke Sun, Tianheng Cheng, Borui Jiang, Chaorui Deng, Yang Zhao, Dong Liu, Yadong Mu, Mingkui Tan, Xinggang Wang, et al. Deep high-resolution representation learning for visual recognition. *IEEE transactions on pattern analysis and machine intelligence*, 43(10):3349–3364, 2020.
- Ashish Vaswani, Noam Shazeer, Niki Parmar, Jakob Uszkoreit, Llion Jones, Aidan N Gomez, Łukasz Kaiser, and Illia Polosukhin. Attention is all you need. *Advances in neural information processing systems*, 30, 2017.
- Mennatullah Siam, Sepehr Valipour, Martin Jagersand, and Nilanjan Ray. Convolutional gated recurrent networks for video segmentation. In *2017 IEEE international conference on image processing (ICIP)*, pages 3090–3094. IEEE, 2017.
- Shanchuan Lin, Linjie Yang, Imran Saleemi, and Soumyadip Sengupta. Robust high-resolution video matting with temporal guidance. In *Proceedings of the IEEE/CVF Winter Conference on Applications of Computer Vision*, pages 238–247, 2022.
- Matthew Loper, Naureen Mahmood, and Michael J Black. Mosh: motion and shape capture from sparse markers. *ACM Trans. Graph.*, 33(6):220–1, 2014.
- Gyeongsik Moon, Hongsuk Choi, and Kyoung Mu Lee. Neuralannot: Neural annotator for 3d human mesh training sets. In *Proceedings of the IEEE/CVF Conference on Computer Vision and Pattern Recognition*, pages 2299–2307, 2022.
- Tsung-Yi Lin, Michael Maire, Serge Belongie, James Hays, Pietro Perona, Deva Ramanan, Piotr Dollár, and C Lawrence Zitnick. Microsoft coco: Common objects in context. In *Computer Vision–ECCV 2014: 13th European Conference, Zurich, Switzerland, September 6–12, 2014, Proceedings, Part V 13*, pages 740–755. Springer, 2014.

- Mykhaylo Andriluka, Leonid Pishchulin, Peter Gehler, and Bernt Schiele. 2d human pose estimation: New benchmark and state of the art analysis. In *Proceedings of the IEEE Conference on computer Vision and Pattern Recognition*, pages 3686–3693, 2014.
- Hanbyul Joo, Natalia Neverova, and Andrea Vedaldi. Exemplar fine-tuning for 3d human model fitting towards in-the-wild 3d human pose estimation. In *2021 International Conference on 3D Vision (3DV)*, pages 42–52. IEEE, 2021.
- Angjoo Kanazawa, Jason Y Zhang, Panna Felsen, and Jitendra Malik. Learning 3d human dynamics from video. In *Proceedings of the IEEE/CVF conference on computer vision and pattern recognition*, pages 5614–5623, 2019.
- Ailing Zeng, Lei Yang, Xuan Ju, Jiefeng Li, Jianyi Wang, and Qiang Xu. Smoothnet: A plug-and-play network for refining human poses in videos. In *European Conference on Computer Vision*, pages 625–642. Springer, 2022.
- Michael J Black, Priyanka Patel, Joachim Tesch, and Jinlong Yang. Bedlam: A synthetic dataset of bodies exhibiting detailed lifelike animated motion. In *Proceedings of the IEEE/CVF Conference on Computer Vision and Pattern Recognition*, pages 8726–8737, 2023.
- Hongwen Zhang, Yating Tian, Yuxiang Zhang, Mengcheng Li, Liang An, Zhenan Sun, and Yebin Liu. Pymaf-x: Towards well-aligned full-body model regression from monocular images. *IEEE Transactions on Pattern Analysis and Machine Intelligence*, 2023.
- Jiefeng Li, Siyuan Bian, Chao Xu, Zhicun Chen, Lixin Yang, and Cewu Lu. Hybrik-x: Hybrid analytical-neural inverse kinematics for whole-body mesh recovery. *arXiv preprint arXiv:2304.05690*, 2023b.
- Chun-Han Yao, Jimei Yang, Duygu Ceylan, Yi Zhou, Yang Zhou, and Ming-Hsuan Yang. Learning visibility for robust dense human body estimation. In *European Conference on Computer Vision*, pages 412–428. Springer, 2022.

## A Additional Quantitative Results

### A.1 Comparison with more image-based methods.

Table S1 compares our TAR with image-based and video-based methods on the 3DPW dataset. All methods are trained on the training set of 3DPW and report the best result using either HRNetWang et al. [2020] or ResNet50He et al. [2016] backbones. Image-based methods focus on per-frame accuracy with advanced network design to extract image features, while video-based methods focus on temporal-consistency and use a pretrained backbone provided by Kolotouros et al. [2019a]. Therefore, image-based methods generally achieve better 3D accuracy than their video-based counterparts. In contrast, our TAR designs a new temporal architecture to exploit both global and local image features to achieve both accuracy and temporal-consistency. Our method outperforms image-based methods in metrics of MPJPE, PA-MPJPE and PVE, and achieve comparable ACCEL metric with state-of-the-art video-based methods. The results demonstrate the superiority and effectiveness of our designs for 3D human motion estimation.

### A.2 Trained with extra data.

We trained TAR with BEDLAMBlack et al. [2023], a recently launched synthetic dataset of 3D human motions, to further verify the performance. As shown in Table S2, TAR achieves better performance on 3DPW dataset with BEDLAM, demonstrating the generalization of our method.

Table S1: Comparison to the state-of-the-arts image-based and video-based methods on 3DPW. All methods are trained on the 3DPW training set and report the best results.

	Method	3DPW		
		MPJPE	PA-MPJPE	PVE
image-based	PyMAFZhang et al. [2023]	74.2	45.3	87.0
	PAREKocabas et al. [2021a]	74.5	46.5	88.6
	HybrIKLi et al. [2023b]	72.9	41.8	88.6
	NIKILi et al. [2023a]	71.3	40.6	86.6
	CLIFFLi et al. [2022]	73.5	44.5	-
	ReFitWang and Daniilidis [2023]	65.8	41.0	-
	VisDBYao et al. [2022]	73.5	44.9	85.5
	Virtual MarkerMa et al. [2023]	67.5	41.3	77.9
	FastMETROCho et al. [2022]	73.5	44.6	84.1
video-based	VIBEKocabas et al. [2020]	91.9	57.6	99.1
	MEVALuo et al. [2020]	86.9	54.7	-
	TCMRChoi et al. [2021]	86.5	52.7	102.9
	MAEDWan et al. [2021]	79.1	45.7	92.6
	MPS-NetWei et al. [2022]	84.3	52.1	99.7
	INTYang et al. [2023]	75.6	42.0	87.9
	GLoTShen et al. [2023]	80.7	50.6	96.3
	TAR(Ours)	<b>62.7</b>	<b>40.6</b>	<b>74.4</b>

Table S2: Evaluation: with additional synthetic data from BEDLAM.

Method	MPJPE↓	PA-MPJPE↓	PVE↓	ACCEL↓
TAR	62.7	40.6	74.4	<b>7.7</b>
TAR+BEDLAMBlack et al. [2023]	<b>60.4</b>	<b>38.8</b>	<b>70.7</b>	7.8

## B Additional Ablation Study

### B.1 Size of hidden maps in ConvGRU

TAR use ConvGRU to model the temporal information of high-resolution local feature maps extracted by CNNsHe et al. [2016]Wang et al. [2020]. Specifically, when the input image crops have shape of  $256 \times 256$ , the local feature maps will

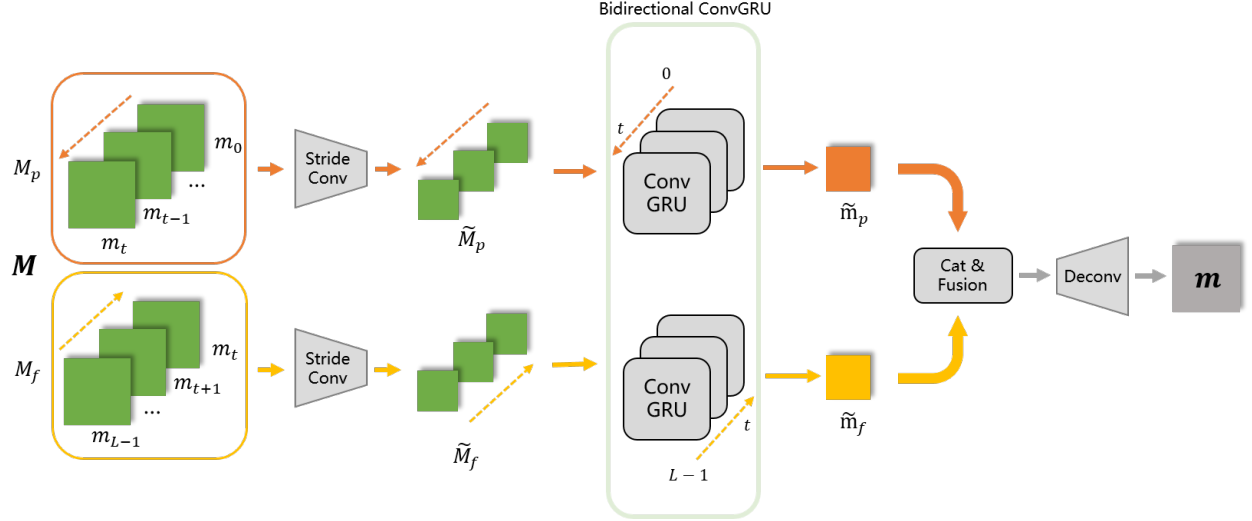


Figure S1: Local Temporal Encoder with downsampled hidden maps.

be  $64 \times 64$ . Although this design is effective for modeling local feature maps, it also brings high computation burdens. In order to reduce the amount of computation and improve the real-time practicality of the model, we provide a variant structure for Local Temporal Encoder as shown in Figure S1. Specifically, we first downsample the local feature maps via a group of strided convolutional layers to reduce the size of hidden maps of ConvGRU. Then the encoded hidden maps  $\tilde{m}_f$  and  $\tilde{m}_p$  are concatenated and fed to deconvolutional layers to restore the feature size. We conduct different downsampling rates to evaluate the impact of hidden feature size of ConvGRU. As shown in Table S3, when the size of hidden maps decreases, the accuracy and smoothness will slightly decrease. In return, the computational complexity is significant reduced. Even with small size of hidden maps (e.g.,  $S=8$ ), TAR still outperforms most state-of-the-art image-based and video-based methods in accuracy and achieves satisfying temporal-consistency.

Table S3: Evaluation of different sizes of ConvGRU hidden maps.  $S$  is the size of hidden maps in ConvGRU.

Method	MPJPE↓	PA-MPJPE↓	PVE↓	ACCE↓L	GFLOPs↓	Params(M)↓
S=64	62.7	40.6	74.4	7.7	184.6	25.0
S=32	65.1	43.4	77.8	8.1	72.4	29.9
S=16	67.3	44.3	81.0	8.5	43.5	34.3
S=8	66.9	43.1	80.1	8.4	36.3	38.5

## C Additional Qualitative Results

We show more comparison results with other methods (TCMRChoi et al. [2021], MPS-NetWei et al. [2022] and GLoTShen et al. [2023]) in Figure S2. Figure ?? gives more test results of EMDB, which contain truncation, occlusion, and challenging poses. FigureS4 shows more challenging internet videos, including dancing and sports scenarios.



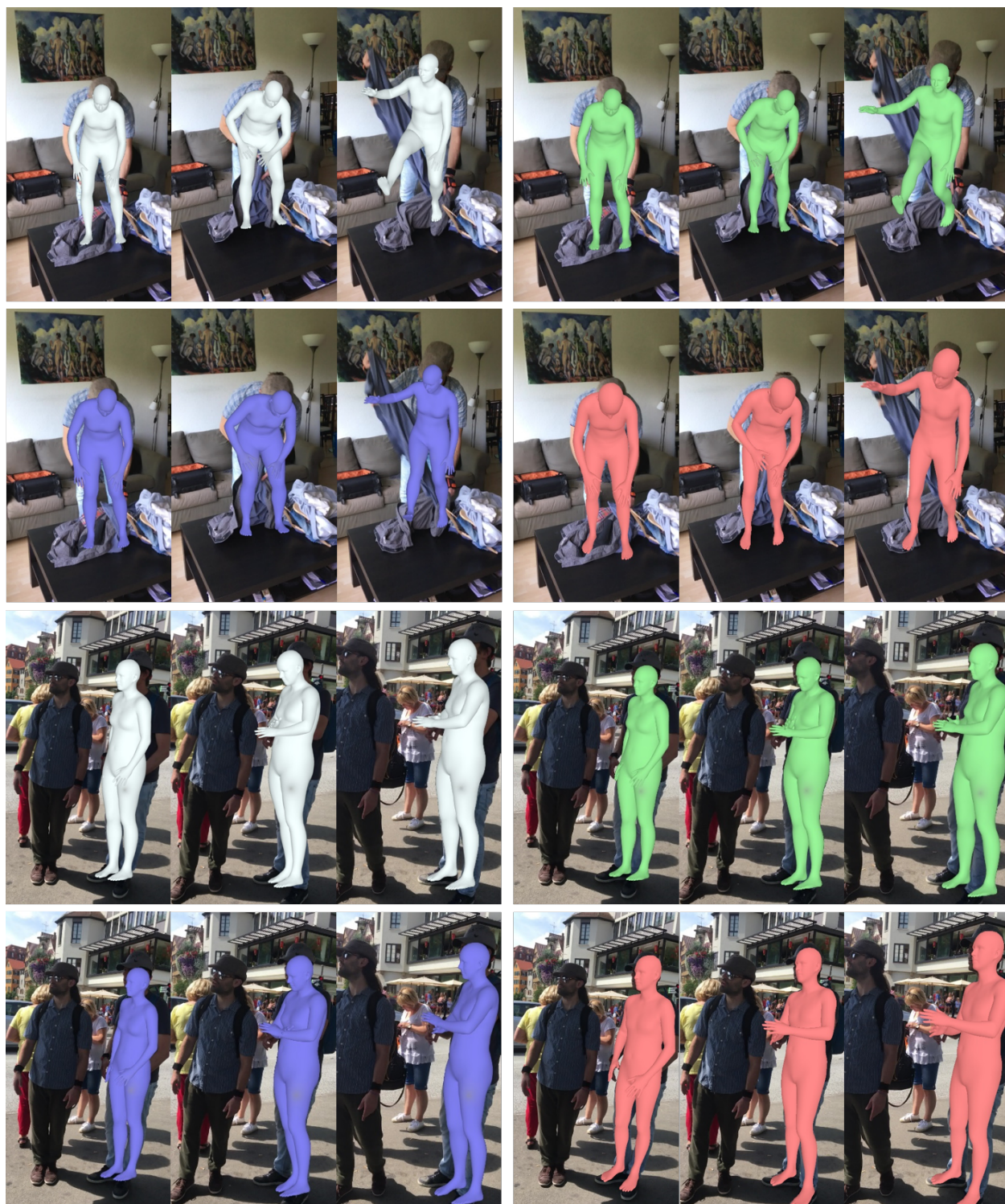


Figure S2: Visual comparison between TCMR, MPS-Net, GLoT and TAR.



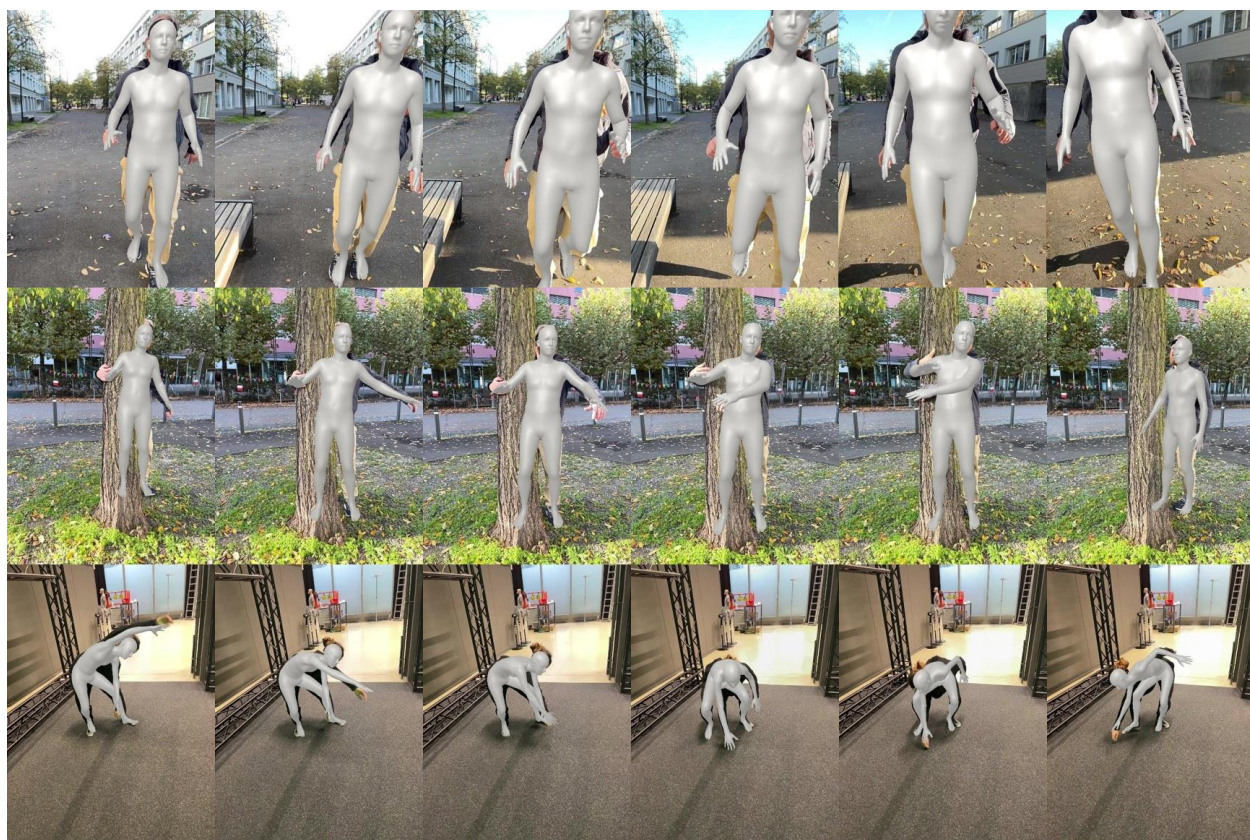


Figure S3: Visual evaluation on EMDBKaufmann et al. [2023] samples.

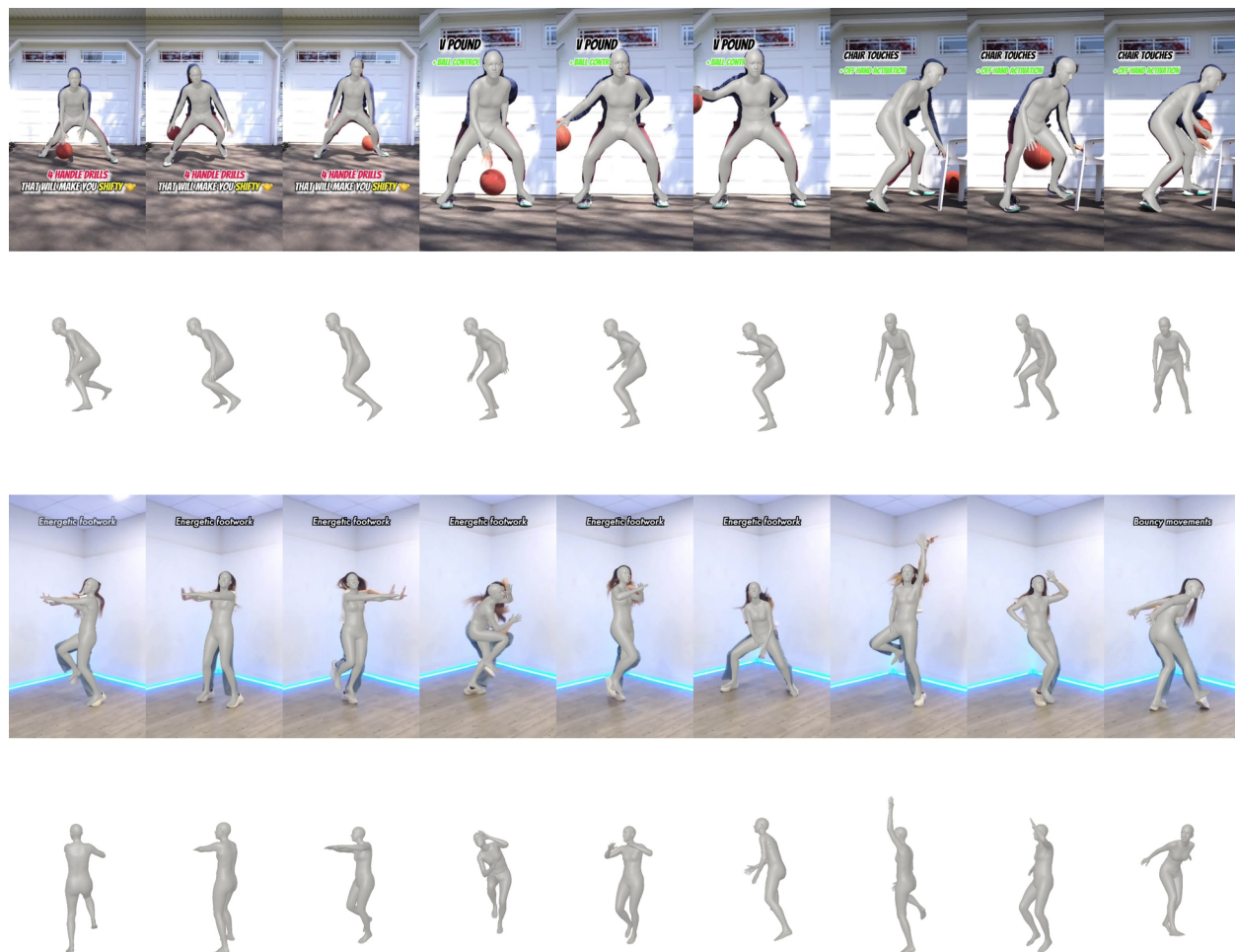


Figure S4: Visual evaluation on internet videos.